

Hadron interferences in the proton induced coherent η meson production reaction on a scalar-isovector nucleus

Swapn Das ¹

*Nuclear Physics Division, Bhabha Atomic Research Centre
Mumbai-400085, India*

Abstract

The coherent η meson energy E_η distribution spectra in the proton nucleus reaction have been calculated to investigate the $\pi^0 - \eta$ mesons' interference, in addition to the study of resonance N^* dynamics in the nucleus. The elementary reaction occurring in the nucleus is assumed to proceed as $pN \rightarrow pN^*$; $N^* \rightarrow N\eta$. Born terms in the intermediate state is also considered. In a scalar-isovector nucleus, this reaction occurs because of π^0 and η meson exchange interactions for the forward going proton and η meson; other meson exchange potentials do not contribute in this process. The sensitivity of the cross section to the hadron nucleus interactions, and the beam energy dependence of the cross section are studied for this reaction.

Keywords: η meson production, hadron interferences

PACS number(s): 25.40e, 13.30.Eg, 13.60.Le

1 Introduction

One of the current interests in the intermediate energy nuclear and particle reactions is to explore the dynamics of η meson which can be produced either in (quasi)bound state or in continuum [1]. Several data sets for the η meson production in the hadron induced reactions are available from various laboratories, like COSY [2] (see the references there in), SATURNE [3], Los Alamos [4], Brookhaven [5]. The production of η meson in heavy-ion collisions was reported from GSI [6]. Due to the advent of high duty electron accelerators at Jefferson Laboratory, Bates, MAMI, ELSA, etc, good quality data have been obtained for the photo- and electro- production of η meson [7]. These accelerator facilities, along with the newly developed sophisticated detecting systems, provide ample scopes to investigate the physics of η meson.

The study of reaction mechanism for the η meson production opens various avenues to learn many exciting physics. Large and attractive ηN scattering length near the threshold production of this meson predicts the existence of a new hadronic atom, i.e., (quasi) η -mesic nucleus [8, 9]. The $\pi^0 - \eta$ mixing is shown to occur in the charge symmetry breaking (CSB) reactions [10]. Being an isoscalar particle, the η meson can excite a nucleon to $I = \frac{1}{2}$

¹Electronic address: swapand@barc.gov.in

resonances. Specifically, $N(1535)$ resonance, $I(J^P) = \frac{1}{2}(\frac{1}{2}^+)$, has large decay branching ratio to η meson and nucleon at the pole mass. Therefore, the η meson production in the nuclear reaction is considered as a potential tool to investigate the dynamics of $N(1535)$ in the nucleus. Of course, this reaction can also be used to study the η meson nucleus interaction in the final state [11, 12].

The η meson can be produced through the hadronic interaction by scattering off the pion or proton on the proton or nuclear target. Theoretical studies of these reactions, as done by various authors [13, 14, 15], show that the η meson in the final state arises because of the decay of $N(1535)$ produced in the intermediate state. Sometime back, Alvaredo and Oset [16] studied the coherent η meson production in the (p, p') reaction on the spin-isospin saturated nucleus: $p + A(gs) \rightarrow p' + A(gs) + \eta$. The elementary reaction in the nucleus is considered as $pN \rightarrow p'N(1535); N(1535) \rightarrow N\eta$. The resonance $N(1535)$ in the intermediate state is produced due to the η meson (a pseudoscalar-isoscalar meson) exchange interaction or potential only, specifically, for the forward going proton and η meson. Contributions from other meson exchange potentials, as discussed in Ref. [16], vanish for this reaction.

The importance of $N(1520)$ resonance in the η meson production reaction is discussed in Ref. [17]. The earlier value of the coupling constant $f_{\eta NN(1520)}$ was 6.72 where as the latest value of it is 9.98. This coupling constant is much larger than the $\eta NN(1535)$ coupling constant: $g_{\eta NN(1535)} \simeq 1.86$. The η meson production cross section due to $N(1520)$ in the above mentioned reaction is increased by a factor of ~ 5 because of the enhancement in $f_{\eta NN(1520)}$. As shown in Fig. 2 of above reference, the $N^* \rightarrow N\eta$ decay probability of $N(1520)$ resonance rises sharply over that of $N(1535)$ with the increase in resonance mass. In fact, this probability for $N(1520)$ is larger than that of $N(1535)$ at higher energy. It is also shown in Ref. [17] that the contribution of $N(1535)$ resonance to the considered reaction is the largest at low energy, i.e., ~ 1 GeV, provided $f_{\eta NN(1520)}$ is taken equal to 6.72. In multi-GeV region, the distinctly dominant contribution to the reaction (quoted above) arises due to $N(1520)$ resonance. In addition to these, the contributions to the cross section due to of Born terms and other resonances (whose $N\eta$ branching ratio is $\geq 4\%$ [18], i.e., $N(1650)$, $N(1710)$ and $N(1720)$ resonances) are also presented in this work.

It should be mentioned that both π and η mesons are pseudoscalar particles but π^0 exchange potential can't contribute to above mentioned reaction since it is an isovector meson and the quoted reaction involves isoscalar nucleus. Contrast to this, both π^0 and η meson exchange interactions can contribute to $p \rightarrow N^*$ excitation in the spin-saturated isovector nucleus. Therefore, the coherent η meson production in the (p, p') reaction on the scalar-isovector nucleus can be used to study the contribution of π^0 and η meson exchange potentials (alongwith their interference) to the reaction. In addition, this reaction can also be used to investigate the dynamics of Born terms and nucleonic resonances, similar

to those presented in Ref. [17].

The diagrammatic presentation of the considered reaction is exhibited in Fig. 1. The upper part of this figure, i.e., Fig. 1(a), describes the direct or post-emission mechanism for the reaction where both Born term N (presented by the bold solid line inside the rectangle box) and resonance term N^* (shown by the rectangle box) have been incorporated. The lower part, i.e., Fig. 1(b), elucidates the cross or post-emission mechanism for the reaction where only Born term N is considered, as the contribution of resonance N^* term in this case can be neglected compared that described in Fig. 1(a) [19].

In the coherent meson production reaction, the meson in the final state, i.e., the η meson in the considered reaction, takes away almost whole energy transferred to the nucleus, i.e., $E_\eta \approx (E_p - E_{p'})$, whereas the momentum of this meson is adjusted by the recoiling nucleus. The state of the nucleus does not change in this reaction. In the formalism for the coherent η meson production in the proton nucleus (scalar-isovector) reaction, the distorted wave functions of protons and η meson are expressed by the eikonal form. The optical potentials (appearing in N^* propagator as well as in distorted wave functions of protons) are worked out using “ $t\rho(\mathbf{r})$ ” approximation. The η meson optical potential is evaluated following that given in Ref. [16]. The cross section for the coherent η meson energy E_η distribution in the above reaction is calculated to study various aspects of it which include (i) the resonance dynamics, (ii) the interference of π^0 and η meson exchange interactions, (iii) the sensitivity of the cross section to the hadron nucleus interaction (optical potential), and (iv) the beam energy dependence of the cross section.

2 Formalism

The Lagrangian \mathcal{L} representing the meson baryon interaction depends on their spin and parity. For the pseudoscalar (0^-) meson (i.e., π or η meson) coupling to the resonances in the considered reaction, \mathcal{L} s are presented below [20, 21]. For the $\frac{1}{2}^+$ particle (i.e., $N(940)$ or $N^* \equiv N(1710)$), they can be expressed as

$$\begin{aligned}
\mathcal{L}_{\pi NN} &= -ig_\pi F_\pi(q^2) \bar{N} \gamma_5 \tau N \cdot \pi \\
\mathcal{L}_{\eta NN} &= -ig_\eta F_\eta(q^2) \bar{N} \gamma_5 N \eta \\
\mathcal{L}_{\pi NN^*} &= -ig_\pi^* F_\pi^*(q^2) \bar{N}^* \gamma_5 \tau N \cdot \pi \\
\mathcal{L}_{\eta NN^*} &= -ig_\eta^* F_\eta^*(q^2) \bar{N}^* \gamma_5 N \eta.
\end{aligned} \tag{1}$$

g_π ($\pi NN(940)$ coupling constant) $\simeq 13.4$ [22], g_η ($\eta NN(940)$ coupling constant) $\simeq 7.93$ [23]; g_π^* ($\pi NN(1710)$ coupling constant) = 1.2, and g_η^* ($\eta NN(1710)$ coupling constant) $\simeq 4.26$. For $\frac{1}{2}^-$ resonance N^* , i.e., $N(1535)$ and $N(1650)$, the forms for \mathcal{L} are given by

$$\mathcal{L}_{\pi NN^*} = -ig_\pi^* F_\pi^*(q^2) \bar{N}^* \tau N \cdot \pi$$

$$\mathcal{L}_{\eta NN^*} = -ig_{\eta}^* F_{\eta}^*(q^2) \bar{N}^* N \eta. \quad (2)$$

$g_{\pi}^* \simeq 0.71$, $g_{\eta}^* \simeq 1.86$ for $N(1535)$ and $g_{\pi}^* \simeq 0.83$, $g_{\eta}^* \simeq 0.67$ for $N(1650)$. For $N(1520)_{\frac{3}{2}^-}$, \mathcal{L} s can be written as

$$\begin{aligned} \mathcal{L}_{\pi NN^*} &= \frac{f_{\pi}^*}{m_{\eta}} F_{\pi}^*(q^2) \bar{N}^{*\mu} \gamma_5 \tau N \cdot \partial_{\mu} \pi \\ \mathcal{L}_{\eta NN^*} &= \frac{f_{\eta}^*}{m_{\eta}} F_{\eta}^*(q^2) \bar{N}^{*\mu} \gamma_5 N \partial_{\mu} \eta. \end{aligned} \quad (3)$$

$f_{\pi}^* = 6.54$ and $f_{\eta}^* \simeq 9.98$. For $\frac{3}{2}^+$ resonance [24], i.e., $N^* \equiv N(1720)$, \mathcal{L} s are given by

$$\begin{aligned} \mathcal{L}_{\pi NN^*} &= \frac{f_{\pi}^*}{m_{\eta}} F_{\pi}^*(q^2) \bar{N}^{*\mu} \tau N \cdot \partial_{\mu} \pi \\ \mathcal{L}_{\eta NN^*} &= \frac{f_{\eta}^*}{m_{\eta}} F_{\eta}^*(q^2) \bar{N}^{*\mu} N \partial_{\mu} \eta. \end{aligned} \quad (4)$$

$f_{\pi}^* \simeq 0.64$ and $f_{\eta}^* \simeq 1.15$. The coupling constants (i.e., g^* s and f^* s) are extracted from the measured decay widths of the resonances, i.e., $N^* \rightarrow N\pi$ and $N^* \rightarrow N\eta$ [18]. $F_{\pi(\eta)}(q^2)$ and $F_{\pi(\eta)}^*(q^2)$ are $\pi(\eta)NN$ and $\pi(\eta)NN^*$ form factors at the respective vertices [23]:

$$F_M(q^2) = F_M^*(q^2) = \frac{\Lambda_M^2 - m_M^2}{\Lambda_M^2 - q^2}; \quad (M \equiv \pi^0, \eta). \quad (5)$$

$q^2 [= q_0^2 - \mathbf{q}^2]$ in this equation is the four-momentum transfer to the nucleus, i.e., $q_0 = E_p - E_{p'}$ and $\mathbf{q} = \mathbf{k}_p - \mathbf{k}_{p'}$. The form factors are normalized to unity when the mesons are in on-shell. Values of the length parameters are $\Lambda_{\pi} = 1.3$ GeV and $\Lambda_{\eta} = 1.5$ GeV [23].

The T -matrix T_{fi} of the considered reaction can be written as

$$T_{fi} = \sum_{M=\pi^0, \eta} [T_B(M) + T_{N^*}(M)], \quad (6)$$

where $T_B(M)$ represents the T -matrix due to Born terms arising because of either π^0 or η meson exchange potential. It is given by

$$T_B(M) = \Gamma_{NN\eta} \Lambda_N(S) V_M(q) \int d\mathbf{r} \chi^{(-)*}(\mathbf{k}_{\eta}, \mathbf{r}) G_N \varrho_I(\mathbf{r}) \chi^{(-)*}(\mathbf{k}_{p'}, \mathbf{r}) \chi^{(+)}(\mathbf{k}_p, \mathbf{r}). \quad (7)$$

The factor ϱ_I in above equation denotes the isospin averaged density distribution of the nucleus. χ s represent the wave functions for the continuum particles. These quantities have been elaborated later. $\Gamma_{NN\eta}$ describes the interaction for the emission of η meson at ηNN vertex in the final state. $V_M(q)$ represents the pseudoscalar meson (i.e., $M \equiv$

Table 1: $\Lambda_{N(N^*)}(S)$ for spin $S = \frac{1}{2}$ and $\frac{3}{2}$ fermions.

Spin(S)	$\Lambda(S)$
$\frac{1}{2}$	$\{\boldsymbol{k} + m_{N^*}\}$
$\frac{3}{2}$	$\{\boldsymbol{k} + m_{N^*}\} \left[g_\nu^\mu - \frac{\gamma^\mu \gamma_\nu}{3} - \frac{\gamma^\mu k_\nu - \gamma^\nu k_\mu}{3m_{N^*}} - \frac{2k^\mu k_\nu}{3m_{N^*}^2} \right]$

π^0 or η) exchange potential between the beam proton and a nucleon in the nucleus, shown by the dash line in Fig. 1: $V_M(q) = \Gamma_{MNN}G_M(q^2)\Gamma_{Mpp'}$. In this equation, Γ_{MNN} denotes the interaction at MNN vertex (in the nucleus) where as $\Gamma_{Mpp'}$ represents that at Mpp' vertex (i.e., meson-projectile-ejectile vertex). These Γ s are addressed by $\mathcal{L}_{\pi(\eta)NN}$ in Eq. (1). $G_M(q^2)$ is the virtual $\pi^0(\eta)$ meson propagator, i.e., $G_{\pi^0(\eta)}(q^2) = -\frac{1}{m_{\pi^0(\eta)}^2 - q^2}$. $\Lambda_N(S)$ represents the spin S dependent part of the nucleon propagator, i.e., $\Lambda_N(S = \frac{1}{2})$ in Table-1. The scalar part of the nucleon Born propagator G_N for direct (D) and cross (C) channels, as illustrated in Fig. 1, are given by

$$G_N^D = \frac{1}{s - m_N^2}; \quad G_N^C = \frac{1}{u - m_N^2}, \quad (8)$$

where s and u are invariant Mandelstam kinematical variables, see page 28 in Ref. [22].

The resonance contribution to T -matrix, i.e., $T_{N^*}(M)$ in Eq. (6), is given by

$$T_{N^*}(M) = \sum_{N^*} \Gamma_{N^* \rightarrow N\eta} \Lambda_{N^*}(S) V_M(q) \int d\mathbf{r} \chi^{(-)*}(\mathbf{k}_\eta, \mathbf{r}) G_{N^*} \varrho_I(\mathbf{r}) \chi^{(-)*}(\mathbf{k}_{p'}, \mathbf{r}) \chi^{(+)}(\mathbf{k}_p, \mathbf{r}). \quad (9)$$

$\varrho_I(\mathbf{r})$ and χ s are also appeared in Eq. (7). $\Gamma_{N^* \rightarrow N\eta}$ denotes $N^* \rightarrow N\eta$ decay in the final state. $V_M(q)$ in this case is given by $V_M(q) = \Gamma_{MNN^*} G_M(q^2) \Gamma_{Mpp'}$, where Γ_{MNN^*} represents the interaction at MNN^* vertex (in the nucleus) described by $\mathcal{L}_{\pi(\eta)NN^*}$ in Eqs. (1 - 4). Other quantities in $V_M(q)$ are already defined below Eq. (7). The spin dependent part of N^* propagator $\Lambda_{N^*}(S)$ is expressed in Table-1. The scalar part of this propagator G_{N^*} in Eq. (9), according to Fig. 1(a), can be expressed as

$$G_{N^*}(m) = \frac{1}{m^2 - m_{N^*}^2 + im_{N^*} \Gamma_{N^*}(m)}, \quad (10)$$

where m_{N^*} are the pole mass of the resonance N^* . $m(\equiv s)$ is the invariant mass of η meson and nucleon, arising due to the decay of N^* . Since the cross or pre-emission channel in this case (as mentioned earlier) can be neglected, it is not considered to evaluate T -matrix. Indeed, this equation represents the resonance propagator in the free space as the resonance nucleus interaction in it (which is considered later) is omitted.

$\Gamma_{N^*}(m)$ in Eq. (23) represents the total width of N^* for its mass equal to m . The experimentally determined value of it at its pole mass, i.e., $m = m_{N^*}$, for all considered resonances are listed in Table-2. Since a resonance N^* can decay into various channels, $\Gamma_{N^*}(m)$ consists of partial decay widths as written below [18].

For $N^* \equiv N(1520)$ resonance,

$$\Gamma_{N^*}(m) = \Gamma_{N^* \rightarrow N\pi}(m)|_{l=2} + \Gamma_{N^* \rightarrow \Delta\pi}(m)|_{l=0} + \Gamma_{N^* \rightarrow \Delta\pi}(m)|_{l=2} + \Gamma_{N^* \rightarrow N\eta}(m)|_{l=2}, \quad (11)$$

where l is the angular momentum associated with the decay. $\Gamma_{N^* \rightarrow N\pi}(m)|_{l=2} \approx 0.65\Gamma_{N^*}(m)$, $\Gamma_{N^* \rightarrow \Delta\pi}(m)|_{l=0} = 0.2\Gamma_{N^*}(m)$, $\Gamma_{N^* \rightarrow \Delta\pi}(m)|_{l=2} = 0.15\Gamma_{N^*}(m)$, $\Gamma_{N^* \rightarrow N\eta}(m)|_{l=2} = 2.3 \times 10^{-3}\Gamma_{N^*}(m)$.

For $N^* \equiv N(1535)$ resonance,

$$\Gamma_{N^*}(m) = \Gamma_{N^* \rightarrow N\pi}(m)|_{l=0} + \Gamma_{N^* \rightarrow N\eta}(m)|_{l=0} + \Gamma_{N^* \rightarrow N\pi\pi}(m); \quad (12)$$

with $\Gamma_{N^* \rightarrow N\pi\pi}(m) = 0.1\Gamma_{N^*}(m_{N^*})$ [25]. $\Gamma_{N^* \rightarrow N\pi}(m)|_{l=0} = 0.48\Gamma_{N^*}(m)$ and $\Gamma_{N^* \rightarrow N\eta}(m)|_{l=0} = 0.42\Gamma_{N^*}(m)$.

For $N^* \equiv N(1650)$ resonance,

$$\Gamma_{N^*}(m) = \Gamma_{N^* \rightarrow N\pi}(m)|_{l=0} + \Gamma_{N^* \rightarrow \Delta\pi}(m)|_{l=2} + \Gamma_{N^* \rightarrow N\eta}(m)|_{l=0}; \quad (13)$$

with $\Gamma_{N^* \rightarrow N\pi}(m)|_{l=0} = 0.75\Gamma_{N^*}(m)$, $\Gamma_{N^* \rightarrow \Delta\pi}(m)|_{l=2} = 0.15\Gamma_{N^*}(m)$ and $\Gamma_{N^* \rightarrow N\eta}(m)|_{l=0} = 0.1\Gamma_{N^*}(m)$.

For $N^* \equiv N(1710)$ resonance,

$$\Gamma_{N^*}(m) = \Gamma_{N^* \rightarrow N\pi}(m)|_{l=1} + \Gamma_{N^* \rightarrow \Delta\pi}(m)|_{l=1} + \Gamma_{N^* \rightarrow N\eta}(m)|_{l=1} + \Gamma_{N^* \rightarrow \Lambda K}(m)|_{l=1}; \quad (14)$$

with $\Gamma_{N^* \rightarrow N\pi}(m)|_{l=1} = 0.2\Gamma_{N^*}(m)$, $\Gamma_{N^* \rightarrow \Delta\pi}(m)|_{l=1} = 0.4\Gamma_{N^*}(m)$, $\Gamma_{N^* \rightarrow N\eta}(m)|_{l=1} = 0.3\Gamma_{N^*}(m)$ and $\Gamma_{N^* \rightarrow \Lambda K}(m)|_{l=1} = 0.1\Gamma_{N^*}(m)$.

For $N^* \equiv N(1720)$ resonance,

$$\Gamma_{N^*}(m) = \Gamma_{N^* \rightarrow N\pi}(m)|_{l=1} + \Gamma_{N^* \rightarrow \Delta\pi}(m)|_{l=1} + \Gamma_{N^* \rightarrow N\eta}(m)|_{l=1} + \Gamma_{N^* \rightarrow \Lambda K}(m)|_{l=1}; \quad (15)$$

with $\Gamma_{N^* \rightarrow N\pi}(m)|_{l=1} = 0.11\Gamma_{N^*}(m)$, $\Gamma_{N^* \rightarrow \Delta\pi}(m)|_{l=1} = 0.75\Gamma_{N^*}(m)$, $\Gamma_{N^* \rightarrow N\eta}(m)|_{l=1} = 0.04\Gamma_{N^*}(m)$ and $\Gamma_{N^* \rightarrow \Lambda K}(m)|_{l=1} = 0.1\Gamma_{N^*}(m)$.

The partial decay width of a resonance N^* decaying to a baryon B and a meson M , i.e., $\Gamma_{N^* \rightarrow BM}(m)|_l$, varies with its mass m [26] as

$$\Gamma_{N^* \rightarrow BM}(m)|_l = \Gamma_{N^* \rightarrow BM}(m_{N^*}) \left[\frac{\Phi_l(m)}{\Phi_l(m_{N^*})} \right]. \quad (16)$$

Table 2: Resonance width $\Gamma_{N^*}(m_{N^*})$ at pole mass m_{N^*} in MeV [18].

Resonance N^*	$\Gamma_{N^*}(m_{N^*})$
$N(1520)$	115
$N(1535)$	150
$N(1650)$	150
$N(1710)$	100
$N(1720)$	250

Table 3: Blatt-Weisskopf barrier-penetration factor $B_l(\tilde{k}R)$ [26].

l	$B_l^2(x = \tilde{k}R)$
0	1
1	$x^2/(1+x^2)$
2	$x^4/(9+3x^2+x^4)$

The phase-space factor $\Phi_l(m)$ is given by $\Phi_l(m) = \frac{\tilde{k}}{m} B_l^2(\tilde{k}R)$, where \tilde{k} is the relative momentum of the decay products (i.e., B and M) in their c.m. frame. $B_l(\tilde{k}R)$ is Blatt-Weisskopf barrier-penetration factor, listed in Table 3. R ($= 0.25$ fm) is the interaction radius.

The five fold differential cross section of the considered reaction can be written as

$$\frac{d\sigma}{dE_{p'}d\Omega_{p'}d\Omega_\eta} = K_F \langle |T_{fi}|^2 \rangle, \quad (17)$$

where the annular brackets around $|T_{fi}|^2$ represent the average over spins in the initial state and the summation over spins in the final state. K_F is the kinematical factor for the reaction:

$$K_F = \frac{\pi}{(2\pi)^6} \frac{m_p^2 m_A k_{p'} k_\eta^2}{k_p |k_\eta (E_i - E_{p'}) - E_\eta \mathbf{q} \cdot \hat{k}_\eta|}. \quad (18)$$

All symbols carry their usual meanings.

3 Results and Discussion

The differential cross sections $\frac{d\sigma}{dE_{p'}d\Omega_{p'}d\Omega_\eta}$ have been calculated for the coherent η meson energy E_η distribution in the (p, p') reaction on ^{14}C , a scalar-isovector nucleus. To describe the plane wave results, χ s in T -matrices in Eqs (7) and (9) are given by $\chi^{(+)}(\mathbf{k}_p, \mathbf{r}) = e^{i\mathbf{k}_p \cdot \mathbf{r}}$ for the beam proton p , and $\chi^{(-)*}(\mathbf{k}_X, \mathbf{r}) = e^{-i\mathbf{k}_X \cdot \mathbf{r}}$ for a particle in the final state, i.e.,

X is either ejectile proton p' or η meson. The resonance nucleus interaction or optical potential $V_{ON^*}(\mathbf{r})$ is not considered at this stage. The spatial density distribution $\varrho(\mathbf{r})$ of ^{14}C nucleus, as extracted from the electron scattering data [27], is given by

$$\varrho(\mathbf{r}) = \varrho_0[1 + w(r/c)^2]e^{-(r/c)^2}; \quad w = 1.38, \quad c = 1.73 \text{ fm.} \quad (19)$$

This density distribution is normalized to the mass number of nucleus.

The isospin averaged nuclear density distribution $\varrho_I(\mathbf{r})$, appearing in Eqs. (7) and (9), is related to $\varrho(\mathbf{r})$ as

$$\varrho_I(\mathbf{r}) = \left[\frac{Z}{A}C_{is}(p) + \frac{(A-Z)}{A}C_{is}(n) \right] \varrho(\mathbf{r}), \quad (20)$$

where $C_{is}(p)$ and $C_{is}(n)$ are the isospin matrix elements for the proton and neutron respectively. $C_{is}(p) = +1$ and $C_{is}(n) = -1$ are the values for π^0 meson exchange potential where as both of them are equal to $+1$ for η meson exchange potential.

The calculated plane wave (V_{ON^*} not included) results at 2.5 GeV are illustrated in Fig. 2. The coherent contribution of π^0 and η meson exchange potentials, i.e., $V_{\pi^0}(q)$ and $V_{\eta}(q)$, are incorporated in these results. This figure represents the cross sections due to Born terms, resonances (mentioned earlier) and that occurring because of their coherent contributions. The dot-dot-dash curve in this figure shows that the cross section because of $N(1520)$ resonance is distinctly largest. Compared to it, the cross sections due to Born terms and other resonances are insignificant. The interferences of Born terms and resonances in the coherently added cross section, presented by dot-dash curve, is visible in the figure. The peak of this cross section arises close to that because of $N(1520)$ resonance.

The cross sections of the considered reaction due to $V_{\pi^0}(q)$ and $V_{\eta}(q)$ at 2.5 GeV is described in Fig. 3. Along with them, the coherently added cross section because of these potentials is also presented in this figure. The upper part of it, i.e., Fig. 3(a), shows the calculated results (plane wave; V_{ON^*} not included) arising due to $N(1520)$ resonance only, since the cross section because of this resonance (as shown in the previous figure) is distinctly largest. The cross section due to V_{π^0} (short-dash curve) is significantly smaller ($\sim \frac{1}{5}$) than that due to V_{η} (large-dash curve). The interference of these potentials is noticeable in the coherently added cross section, see dot-dot-dash curve in this figure.

The smaller cross section arising because of π^0 meson exchange potential V_{π^0} over that due to η meson exchange potential V_{η} may be understood, as an initial thought, by analyzing the ratios of various factors appearing in $\left| \frac{V_{\pi^0}}{V_{\eta}} \right|^2$ at the respective peak of the cross sections. The coupling constants, quoted below Eqs. (1) and (3), show the ratio $\left| \frac{g_{\pi}f_{\pi}^*}{g_{\eta}f_{\eta}^*} \right|^2$ is approximately equal to 1.23. The ratio of isospin matrix elements in $\left| \frac{V_{\pi^0}(q)}{V_{\eta}(q)} \right|^2$ is $\frac{1}{49}$, as

the isospin contribution of a proton cancels that of a neutron in the nucleus for $V_{\pi^0}(q)$. Referring to Fig. 3(a), the peak cross section due to $V_{\pi^0}(q)$ appears at the four-momentum transfer $q^2 \simeq -0.18 \text{ GeV}^2$ where as that because of $V_{\eta}(q)$ arises at $q^2 \approx -0.25 \text{ GeV}^2$. The form factors at the respective peaks, according to Eq. (5), are $F_{\pi}(q^2 \simeq -0.18 \text{ GeV}^2) = F_{\pi}^*(q^2 \simeq -0.18 \text{ GeV}^2) \simeq 0.89$ and $F_{\eta}(q^2 \approx -0.25 \text{ GeV}^2) = F_{\eta}^*(q^2 \approx -0.25 \text{ GeV}^2) \simeq 0.78$. These values give $\left|\frac{F_{\pi}(q^2)}{F_{\eta}(q^2)}\right|^4 \simeq 1.7$. The values of the pseudoscalar meson propagators are $G_{\pi}(q^2 \simeq -0.18 \text{ GeV}^2) \simeq -5.06 \text{ GeV}^{-2}$ and $G_{\eta}(q^2 \approx -0.25 \text{ GeV}^2) \approx -1.83 \text{ GeV}^{-2}$, which show $\left|\frac{G_{\pi}(q^2)}{G_{\eta}(q^2)}\right|^2 \approx 7.65$. The product of these factors shows $\left|\frac{V_{\pi^0}(q)}{V_{\eta}(q)}\right|^2 \simeq \frac{1}{3.06}$. But, the calculated results show the peak cross section due to V_{η} is ~ 5 larger than that because of V_{π^0} .

To resolve the above discrepancy (i.e., a factor of ~ 1.63), the $N^*(m) \rightarrow N\eta$ decay probabilities (for $N^* \equiv N(1520)$) at the peaks quoted in the previous analysis are considered. It is noticeable in Fig. 3(a) that the peak cross section because of V_{π^0} appears at $E_{\eta} \simeq 1.18 \text{ GeV}$ which corresponds to the resonance mass $m \approx 1.83 \text{ GeV}$, as mentioned on the upper x-axis of this figure. The peak of the cross section because of V_{η} appears at $m \simeq 1.9 \text{ GeV}$. The ratio of the decay probabilities at the respective peaks $\frac{\Gamma_{N^* \rightarrow N\eta}(m \approx 1.83 \text{ GeV})|_{V_{\pi^0}}}{\Gamma_{N^* \rightarrow N\eta}(m \approx 1.9 \text{ GeV})|_{V_{\eta}}}$, according to Eq. (16), is close to $\frac{1}{1.61}$. Therefore, the above analyses justify the lesser cross section due to V_{π^0} over that because of V_{η} , as visible in Fig. 3(a).

The importance of V_{π^0} and V_{η} in the coherently added cross sections due to Born terms and quoted resonances are presented in Fig. 3(b). These spectra show features which are qualitatively similar to those elucidated in the upper part of this figure. This occurs since the distinctly dominant cross section, as mentioned earlier, arises because of $N(1520)$ resonance.

To include the hadron nucleus interaction (optical potential) in the calculated cross section, the distorted wave functions are used for χ s in T -matrices (given in Eqs (7) and (9)) and G_{N^*} in Eq. (10) is replaced by the in-medium resonance propagator. Using Glauber model [28, 29], χ for beam proton p can be written as

$$\chi^{(+)}(\mathbf{k}_p, \mathbf{r}) = e^{i\mathbf{k}_p \cdot \mathbf{r}} \exp\left[-\frac{i}{v_p} \int_{-\infty}^z dz' V_{Op}(\mathbf{b}, z')\right]. \quad (21)$$

For outgoing particles, i.e., p' and η meson, the form for the distorted wave functions is

$$\chi^{(-)*}(\mathbf{k}_X, \mathbf{r}) = e^{-i\mathbf{k}_X \cdot \mathbf{r}} \exp\left[-\frac{i}{v_X} \int_z^{+\infty} dz' V_{OX}(\mathbf{b}, z')\right]; \quad (X = p', \eta). \quad (22)$$

v and $V(\mathbf{b}, z')$ in above equations represent the velocity and optical potential respectively of the continuum particle. These potentials describe the initial and final state interactions of the reaction.

Incorporating the resonance nucleus interaction $V_{ON^*}(\mathbf{r})$ in $G_{N^*}(m)$ given in Eq. (10), the resonance propagator in the nucleus can be expressed as

$$G_{N^*}(m, \mathbf{r}) = \frac{1}{m^2 - m_{N^*}^2 + im_{N^*}\Gamma_{N^*}(m) - 2E_{N^*}V_{ON^*}(\mathbf{r})}, \quad (23)$$

where E_{N^*} is the energy of the resonance N^* .

The optical potential $V_{OX}(\mathbf{r})$, appearing in Eqs. (21) - (23), is calculated using “ $t\rho(\mathbf{r})$ ” approximation [29], i.e.,

$$V_{OX}(\mathbf{r}) = -\frac{v_X}{2}[i + \alpha_{XN}]\sigma_t^{XN}\rho(\mathbf{r}), \quad (24)$$

where the symbol X represents either a proton or a resonance N^* . v_X is the velocity of the particle X . α_{XN} denotes the ratio of the real to imaginary part of X -nucleon scattering amplitude f_{XN} , and σ_t^{XN} is the corresponding total cross section. To evaluate the proton nucleus optical potential, i.e., $V_{Op}(\mathbf{r})$ as well as $V_{Op'}(\mathbf{r})$, the energy dependent experimentally determined values for α_{pN} and σ_t^{pN} have been used [30]. The measured values for N^* -nucleon scattering parameters, i.e., α_{N^*N} and $\sigma_t^{N^*N}$, are not available. To estimate them, $\alpha_{N^*N} \approx \alpha_{pN}$ and $\sigma_{el}^{N^*N} \approx \sigma_{el}^{pN}$ are taken since the elastic scattering dynamics of N^* can be assumed not much different from that of a proton [31]. For the reactive part of $\sigma_t^{N^*N}$, the dynamics of N^* can be considered same as that of a nucleon at its kinetic energy enhanced by Δm , i.e., $\sigma_r^{N^*N}(T_{N^*N}) \approx \sigma_r^{NN}(T_{N^*N} + \Delta m)$. Here, Δm is the mass difference between the resonance and nucleon. T_{N^*N} is the total kinetic energy in the N^*N center of mass system [31].

The η meson optical potential $V_{O\eta}(\mathbf{r})$ is evaluated from its self-energy $\Pi_\eta(\mathbf{r})$ in the nucleus. The resonance hole contribution to $\Pi_\eta(\mathbf{r})$, according to Alvaredo and Oset [16], can be written as

$$\Pi_\eta(\mathbf{r}) = 2E_\eta V_{O\eta}(\mathbf{r}) = \sum_{N^*} |C(N^*)|^2 \frac{\rho(\mathbf{r})}{m - m_{N^*} + \frac{i}{2}\Gamma_{N^*}(m) - V_{ON^*}(\mathbf{r}) + V_{ON}(\mathbf{r})}. \quad (25)$$

The prefactor $|C(N^*)|^2$ in this equation depends on N^* used to evaluate $\Pi_\eta(\mathbf{r})$. The nucleon potential energy in the nucleus is taken as $V_{ON}(\mathbf{r}) = -50\rho(\mathbf{r})/\rho(0)$ MeV [16]. $\Pi_\eta(\mathbf{r})$ arising due to nucleon hole pair is worked out following that due to π^0 meson, see page 157 in Ref. [22].

The sensitivity of the calculated cross section to the hadron nucleus interaction is exhibited in Fig. 4. The large peak (shown in this figure) in the coherently added cross sections (arising because of Born terms and considered resonances as well as because of π^0 and η meson exchange potentials) is considered for this purpose. The dot-dash curve represents the plane wave (V_{ON^*} not included) cross section of the considered reaction (also shown earlier). The cross section is reduced by a factor of 3.74 because of the

incorporation of initial state interaction (ISI), see the long-dash curve. The short-dash curve elucidates the calculated spectrum obtained after the inclusion of both ISI and FSI (final state interaction), i.e., it describes the distorted wave results where V_{ON^*} is not taken into consideration. The cross section is further reduced by a factor of 2.86 due to the inclusion of FSI. The solid curve represents the calculated distorted wave results where V_{ON^*} has been incorporated. It shows the change in the cross section due to this potential is negligible. Therefore, the calculated plane wave (V_{ON^*} not included) cross section is reduced drastically, i.e., by a factor of 11.81, because of the inclusion of all hadron nucleus interactions. The shift in the peak position because of these interactions is about 40 MeV towards the higher value of E_η in the spectrum.

The beam energy dependence of the distorted wave results are elucidated in Fig. 5. The resonance nucleus interactions are also included in this results. The cross section at the large peak is increased by a factor of 5.37, and the peak position is shifted from $E_\eta \simeq 1.39$ GeV to $E_\eta \simeq 1.75$ GeV with the increase in the beam energy from 2.25 GeV to 3 GeV.

4 Conclusions

The differential cross sections have been calculated for the coherent η meson energy E_η distribution in the proton induced reaction on the scalar-isovector nucleus. The η meson in the final state is considered to arise because of Born terms and resonances produced in the intermediate state. The interaction between the projectile proton and a nucleon in the target nucleus is described by the pseudoscalar meson, i.e., π^0 and η mesons, exchange potentials. The calculated results show that the distinctly dominant contribution to the η meson production cross section arises because of $N(1520)$ resonance. The coherently added cross section arising due to Born terms and considered resonances is less than the previous due to their interferences. The cross section because of π^0 meson exchange potential is lesser than that due to η meson exchange potential. The interference of these potentials is distinctly visible in the η meson energy E_η distribution spectrum. The cross section is reduced drastically and shifted towards higher E_η because of the hadron nucleus interactions, i.e., initial and final state interactions including resonance nucleus interactions. The calculated results show that the cross section is very sensitive to the beam energy, as the magnitude of cross section increases and its peak position shifts towards higher E_η with the enhancement in the beam energy.

5 Acknowledgement

The author thanks the anonymous referee for giving the comments which improved the quality of this work. Dr. L. M. Pant is acknowledged for his help in editing the manuscript.

References

- [1] V. Baru et al., arXiv/nucl-th:0610011.
- [2] S. Schadmand (for WASA at COSY Collaboration), *Pramana* **75** (2010) 225.
- [3] J. Berger et al., *Phys. Rev. Lett.* **61** (1988) 919; R. Frascaria et al., *Phys. Rev. C* **50** (1994) R537.
- [4] J. C. Peng et al., *Phys. Rev. Lett.* **63** (1989) 2353.
- [5] W. B. Tippens et al., *Phys. Rev. D* **63** (2001) 052001.
- [6] F. -D. Berg et al., *Phys. Rev. Lett.* **72** (1994) 977.
- [7] M. Williams et al., *Phys. Rev. C* **80** (2009) 045213; B. Krusche et al., *Phys. Rev. Lett.* **74** (1995) 3736; J. W. Price et al., *Phys. Rev. C* **51** (1995) 2283(R); B. Krusche et al., *Phys. Lett. B* **358** (1995) 40; M. Rößig-Landau et al., *Phys. Lett. B* **373** (1996) 45.
- [8] R. S. Bhalerao and L. -C. Liu, *Phys. Rev. Lett.* **54** (1985) 865; Q. Haider and L. -C. Liu, *Phys. Lett. B* **172** (1986) 257; L. -C. Liu and Q. Haider, *Phys. Rev. C* **34** (1986) 1845; G. L. Li, W. K. Cheng and T. T. S. Kuo, *Phys. Lett. B* **195** (1987) 515.
- [9] R. E. Chrien et al., *Phys. Rev. Lett.* **60** (1988) 2595; A. Budzanowski et al., (COSY-GEM Collaboration), *Phys. Rev. C* **79** (2009) 012201(R).
- [10] C. Y. Cheung, *Phys. Lett. B* **119** (1982) 47; C. Wilkin, *Phys. Lett. B* **331** (1994) 276.
- [11] J. Lehr, M. Post and U. Mosel, *Phys. Rev. C* **68** (2003) 044601; J. Lehr and U. Mosel, *ibid*, 044603; R. C. Carrasco, *ibid*, **48** (1993) 2333.
- [12] M. Hedayati-Poor and H. S. Sherif, *Phys. Rev. C* **76** (2007) 055207; M. Hedayati-Poor, S. Bayegan and H. S. Sherif, *Phys. Rev. C* **68** (2003) 045205.
- [13] Ch. Sauerma, B. L. Friman and W. Nörenberg, *Phys. Lett. B* **341** (1995) 261; J. -F. Germond and C. Wilkin, *Nucl. Phys. A* **518** (1990) 308; A. Moalem, E. Gedalin, L. Razdolskaja and Z. Shorer, *Nucl. Phys. A* **589** (1995) 649.
- [14] J. M. Laget, F. Wellers and J. F. Lecolley, *Phys. Lett. B* **257** (1991) 254.
- [15] T. Vetter, A. Engel, T. Brió and U. Mosel, *Phys. Lett. B* **263** (1991) 153.

- [16] B. López Alvaredo and E. Oset, Phys. Lett. B **324** (1994) 125.
- [17] Swapan Das, Phys. Lett. B **737** (2014) 75.
- [18] J. Beringer et al., Particle Data Group, Phys. Rev. D **86** (2012) 010001.
- [19] L. -C. Liu, J. T. Londergan, and G. E. Walker, Phys. Rev. C **40** (1989) 832.
- [20] W. Peters, H. Lenske and U. Mosel, Nucl. Phys. A **642** (1998) 506.
- [21] I. R. Blokland and H. S. Sherif, Nucl. Phys. A **694** (2001) 337.
- [22] T. Ericson and W. Weise, Pions and Nuclei (Clarendon Press, Oxford, 1988), p. 18.
- [23] H. C. Chiang, E. Oset and L. -C. Liu, Phys. Rev. C **44** (1991) 738; R. Machleidt, K. Holinde and Ch. Elster, Phys. Rep. **149** (1987) 1.
- [24] Swapan Das, Phys. Rev. C **70** (2004) 034604.
- [25] G. Fäldt and C. Wilkin, Nucl. Phys. A **587** (1995) 769; A. Fix and H. Arenhövel, Nucl. Phys. A **620** (1997) 457.
- [26] D. M. Manley, R. A. Arndt, Y. Goradia and V. I. Teplitz, Phys. Rev. D **30** (1984) 904; D. M. Manley, Phys. Rev. D **51** (1995) 4837; *ibid*, Int. J. Mod. Phys. A **18** (2003) 441.
- [27] C. W. De Jager, H. De. Vries and C. De Vries, At. Data Nucl. Data Tables, **14** (1974) 479.
- [28] R. J. Glauber, in Lectures in theoretical physics, vol. 1, edited by W. E. Brittin et al., (Interscience Publishers, New York, 1959).
- [29] Swapan Das, Phys. Rev. C **72** (2005) 064619.
- [30] D. V. Bugg, et al., Phys. Rev. **146** (1966) 980; S. Barshay, et al., Phys. Rev. C **11** (1975) 360; W. Grein, Nucl. Phys. B **131** (1977) 255; C. Lechanoine-Leluc and F. Lehar, Rev. Mod. Phys. **65** (1993) 47; R. M. Barnett et al., Particle Data Group, Phys. Rev. D **54**, (1996) 192; <http://pdg.lbl.gov/xsect/contents.html>.
- [31] B. K. Jain, N. G. Kelkar and J. T. Londergan, Phys. Rev. C **47** (1993) 1701.

Figure Captions

1. (color online). Schematic diagrams describing the mechanism of the considered reaction (see text): (a) direct (or post-emission) and (b) cross (or pre-emission) diagrams.
2. (color online). The η meson energy E_η distribution spectra for ^{14}C nucleus at 2.5 GeV. The cross section due to $N(1520)$ resonance is distinctly largest (dot-dot-dash curve). The coherently added cross section (dot-dash curve) is less than the previous because of the interference of Born terms and resonances quoted in the figure.
3. (color online). Upper part: Contributions of π^0 and η meson exchange potentials to the cross section arising due to $N(1520)$ resonance only. The peak position is shifted to the higher value of E_η because of the interference of these potentials (dot-dot-dash curve). Lower part: Same as those presented in the upper part but for the coherently added cross sections due to Born terms and resonances (see text).
4. (color online). The sensitivity of the cross section to the hadron nucleus interaction (optical potential). The cross section is reduced drastically (by a factor of $\simeq 12$), and the peak position is shifted by 40 MeV towards the higher value of E_η because of these interactions.
5. (color online). Beam energy dependence of the cross section. The cross section increases and the peak position shifts towards the higher E_η with the enhancement in the beam energy.

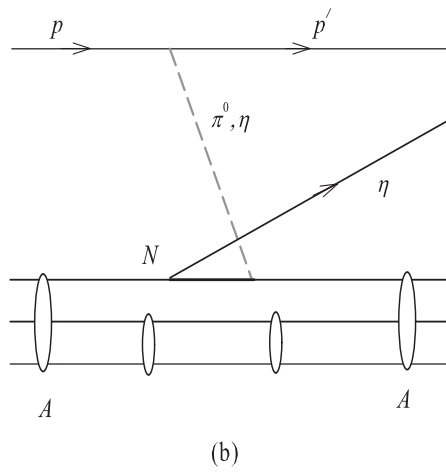
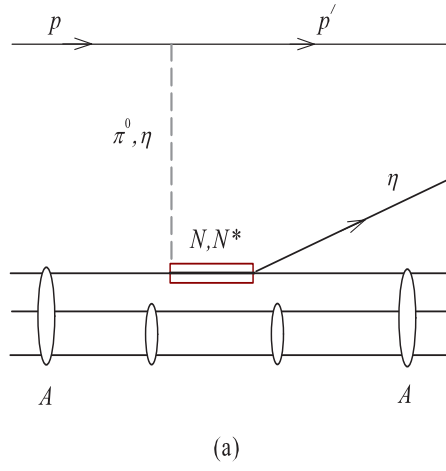


Figure 1: (color online). Schematic diagrams describing the mechanism of the considered reaction (see text): (a) direct (or post-emission) and (b) cross (or pre-emission) diagrams.

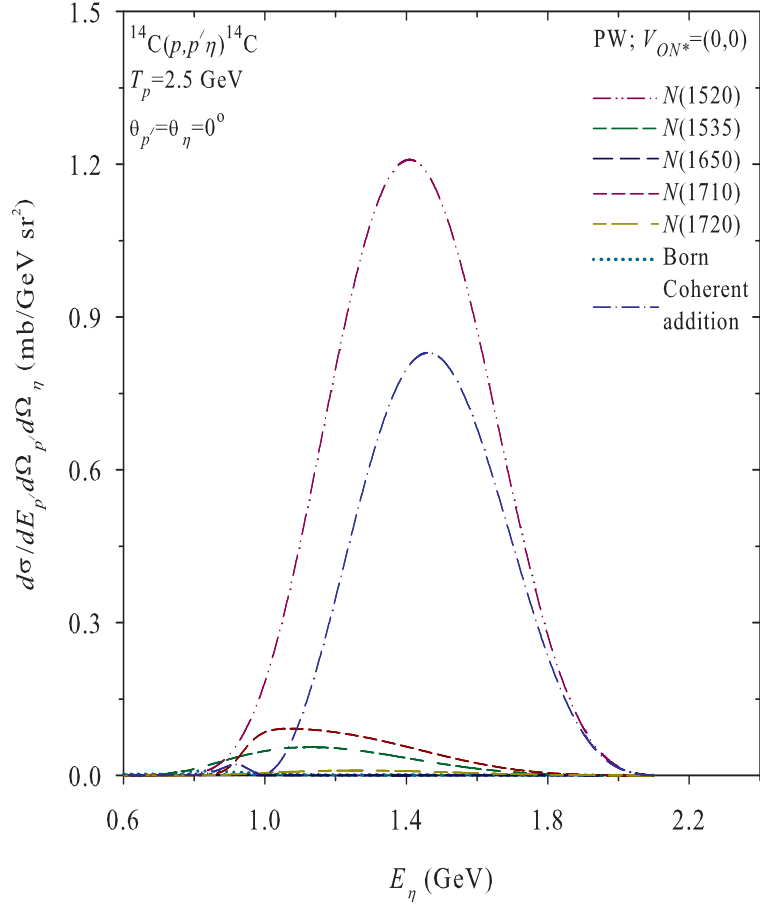


Figure 2: (color online). The η meson energy E_η distribution spectra for ^{14}C nucleus at 2.5 GeV. The cross section due to $N(1520)$ resonance is distinctly largest (dot-dot-dash curve). The coherently added cross section (dot-dash curve) is less than the previous because of the interference of Born terms and resonances quoted in the figure.

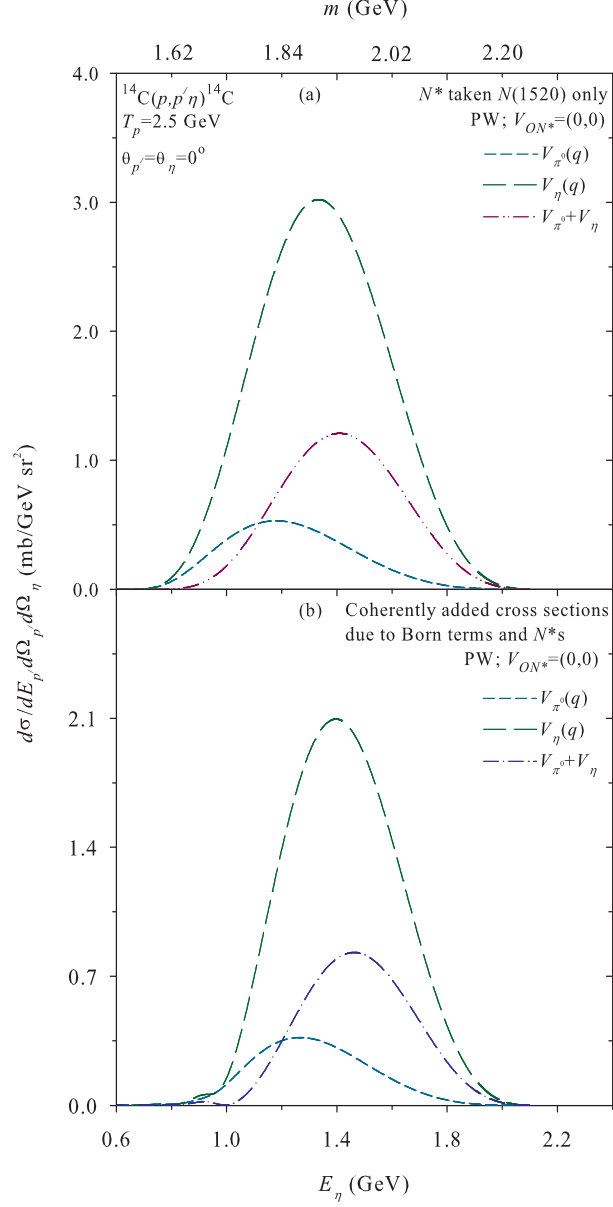


Figure 3: (color online). Upper part: Contributions of π^0 and η meson exchange potentials to the cross section arising due to $N(1520)$ resonance only. The peak position is shifted to the higher value of E_η because of the interference of these potentials (dot-dot-dash curve). Lower part: Same as those presented in the upper part but for the coherently added cross sections due to Born terms and resonances (see text).

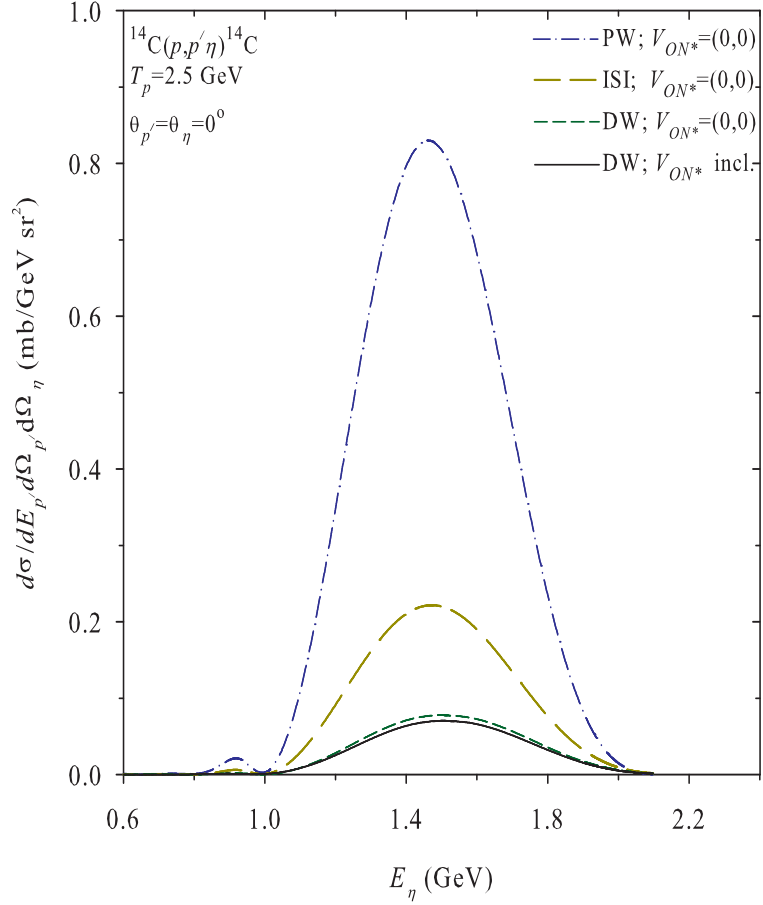


Figure 4: (color online). The sensitivity of the cross section to the hadron nucleus interaction (optical potential). The cross section is reduced drastically (by a factor of $\simeq 12$), and the peak position is shifted by 40 MeV towards the higher value of E_η because of these interactions.

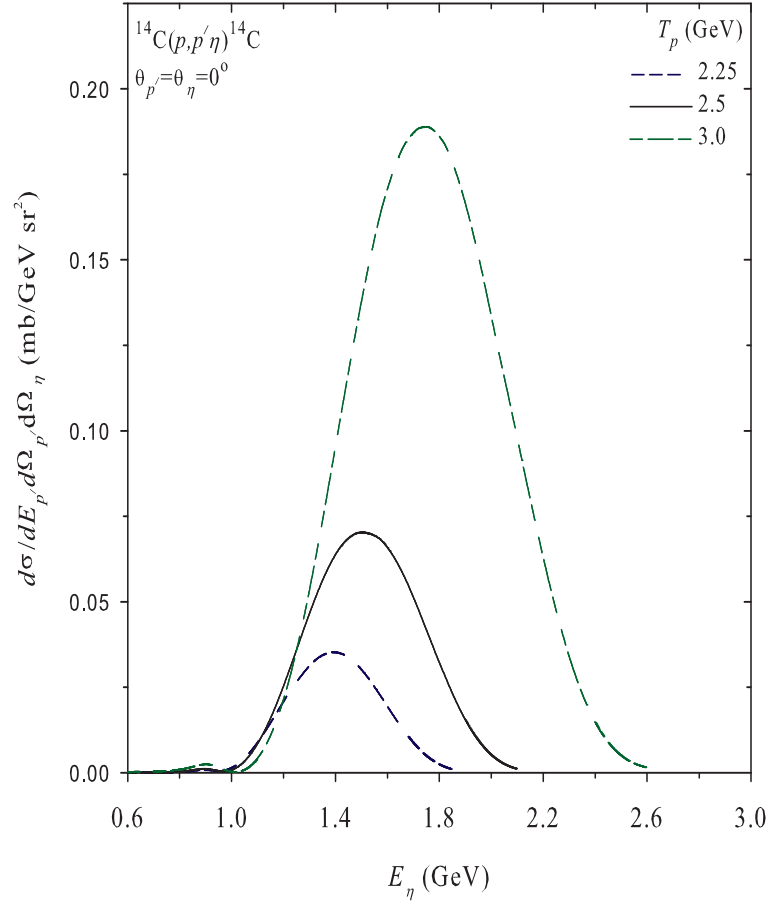


Figure 5: (color online). Beam energy dependence of the cross section. The cross section increases and the peak position shifts towards the higher E_{η} with the enhancement in the beam energy.